Spectral broadband dynamics of semiconductor lasers with resonant short cavities

Michael Peil,* Ingo Fischer,† and Wolfgang Elsäßer‡
Institute of Applied Physics, Darmstadt University of Technology, Schloßgartenstraße 7, 64289 Darmstadt, Germany
(Received 11 November 2005; published 6 February 2006)

We present a semiconductor laser system tailored to exhibit unusual spectral broadband emission dynamics. We study the dynamics properties and its physical origin in detail and discuss the potential of this system as a high-power incoherent laser light source. Our semiconductor laser (SL) system comprises a particularly long edge-emitting laser of 1.6 mm length and a short external cavity of comparable length. We have adjusted for resonant coupling conditions between both cavities, such introducing strong modal coupling. By varying the pumping or the optical feedback phase, we obtain a characteristic cyclic scenario evolving from stable emission via a period-doubling cascade to chaos and back to stable emission. We find distinct differences to the short-cavity regime of conventional nonresonant SL systems reported so far. The most prominent difference is the onset of chaotic intensity dynamics in conjunction with pronounced multimode dynamics of high optical bandwidth exceeding ~7 nm, therefore comprising more than 100 lasing longitudinal modes. In that sense, the presented system represents an excellent nonlinear dynamical model system offering well-controllable generation of distinct multimode dynamics. Furthermore, we demonstrate that the nonlinear dynamics properties allow for controlled adjustment of the coherence length in a wide range between ~130 μm and ~8 m. This property facilitates application in novel measurement technology in which (in)coherence properties are of importance.

DOI: 10.1103/PhysRevA.73.023805 PACS number(s): 42.65.Sf, 05.45.Jn, 05.45.Gg, 42.55.Px

I. INTRODUCTION

In recent years, the dynamics of semiconductor lasers (SLs) with delayed optical feedback has attracted much attention in the field of nonlinear dynamics (NLD). From the fundamental NLD point of view, these SL systems are interesting model systems because their emission dynamics exhibit numerous intriguing phenomena [1] including high-dimensional chaos. On the one hand, the rich dynamical qualities of SLs with delayed optical feedback can be attributed to the fact that they belong to the class of delay systems. Delay systems are mathematically infinite dimensional, offering potential for the emergence of high-dimensional dynamics. On the other hand, SLs exhibit a substantial inherent nonlinearity originating from strong interactions of the intense light field and the gain material inside the SL cavity which is often phenomenologically described by the α parameter [2]. This linkage of delayed feedback and the strong nonlinearity is an ideal premise for the occurrence of high-dimensional chaotic intensity dynamics in conjunction with pronounced spectral dynamics and, eventually, gives rise to the multitude of dynamical phenomena which have been observed. To date, several fundamental dynamics phenomena occurring in delay systems are still not fully understood. Since analytical treatment of delay systems is very demanding, complementary experimental access to the problem is desired. In this context, well-controllable SL systems with delayed feedback represent established model systems for experimental studies on fundamental NLD phenomena of delay systems, which already have significantly contributed to today's understanding of the classical routes to chaos, i.e., via intermittency [3], bifurcation cascades [4], period doubling [5], and quasiperiodicity [5,6]. Insight into the fundamental mechanisms determining the dynamics properties of SL systems, in turn, allows for controlled manipulation of the nonlinear dynamics. Therefore, NLD can be harnessed for tailoring the emission properties of SLs. In particular, the controlled generation of high-dimensional, broadband chaotic emission dynamics offers perspectives for novel chaos-based technologies, e.g., for chaotic light detection and ranging (CLIDAR) [7] or encrypted communications [8,9].

So far, research has mainly focused on systems with external cavities L_{EC} being sufficiently longer than the semiconductor laser cavity L_{SL} [10–14]. It has turned out that most of the dynamics of these systems is captured by models based on the Lang-Kobayashi (LK) SL rate equations [14–16]. For that reason, the LK equations have become an established basis for modeling SL systems. However, derivation of the LK equations is based on several assumptions and simplifications which are not fulfilled in general. Two main assumptions of this mean-field model are the consideration of only one (single) longitudinal SL mode and the neglect of the longitudinal extension of the semiconductor laser cavity. However, in some SLs, further modes and spatial dependencies can become important. To capture modal dynamics, for instance, extended versions of the LK equations have been proposed which account for emission of multiple coupled longitudinal SL modes. In one class of these LK-based models, each longitudinal mode (LM) is considered by one field equation, while all LMs deplete the shared carrier reservoir. In these models, the LMs are either coupled through self-interaction and cross-interaction processes [17,18] or a

*Electronic address: michael.peil@physik.tu-darmstadt.de
†Present address: Department of Applied Physics and Photonics, Vrije Universiteit Brussel, B-1050 Brussels, Belgium. Electronic address: ifischer@tona.vub.ac.be
‡Electronic address: elsaesser@physik.tu-darmstadt.de

mode-dependent gain is considered [19]. In the second class of LK multimode models, in spirit of the Tang-Statz-deMars [20] model, in additional to the extra field equations, different carrier densities are assumed for each mode [21–23]. In the past years, these diverse models have substantially contributed to today's understanding of dynamics phenomena which are caused by multimode interactions [24,25]. However, these models are also based on assumptions which determine limits of validity preventing general applicability. A promising and powerful alternative is provided by traveling wave models, which can account for multimode dynamics and spatial effects [26–31]. Unfortunately, this approach is mathematically demanding, impeding physical interpretation of the results.

In this work, we will demonstrate that SL systems with properties beyond validity of the conventional LK description can reveal interesting dynamics phenomena including distinct multimode emission dynamics. Therefore, these systems can provide essential insight into the properties of complex nonlinear multimode systems in general. In addition, the intriguing characteristics of the emission properties of these systems can be harnessed for realization of novel technical applications which are based on utilization of chaotic light. In this context, we present a distinguished multimode external cavity SL system which clearly violates fundamental assumptions of LK modeling, i.e., single LM emission and neglect of the longitudinal extension of the semiconductor laser cavity. In contrast to conventional LK systems, the lengths of the external cavity L_{EC} and the length of the semiconductor laser cavity L_{SL} are of comparable size. For these conditions, the longitudinal extension of the SL cavity becomes important for the dynamics. This becomes evident when we additionally introduce resonance conditions between the two cavities to enhance the coupling between the LMs. As we will demonstrate, the combination of both features can trigger excitation of numerous strongly interacting LMs manifesting in extraordinarily high optical bandwidth, if compared to conventional external cavity SL systems. Because of this striking difference, the main focus of this work is dedicated to the emergence and analysis of the fascinating multimode dynamics exhibited by this SL system.

The paper is organized as follows. In Sec. II, we introduce the resonant short cavities SL system and describe the experimental setup which we utilize for characterization of its dynamics. In Sec. III, we demonstrate how coupling between the LMs can be distinctly enhanced for the resonant cavities conditions. In Sec. IV, we study the influence of the relevant system parameters on the dynamics, which are the pump parameter and the feedback phase. For variation of both parameters, we find a cyclic scenario in which the dynamics evolve from stable emission, via periodic states, to chaos, and subsequently back to stable emission. We show that for high pump parameters, we are able to achieve broadband chaotic intensity dynamics for which the number of LMs being involved in this dynamics can easily exceed 100. We analyze the emergence of this extraordinary optical broadband dynamics disclosing the strong interrelation between intensity and spectral dynamics. Analysis of the coherence properties of this dynamics elucidates the high potential of this light source in terms of modern technical applications.

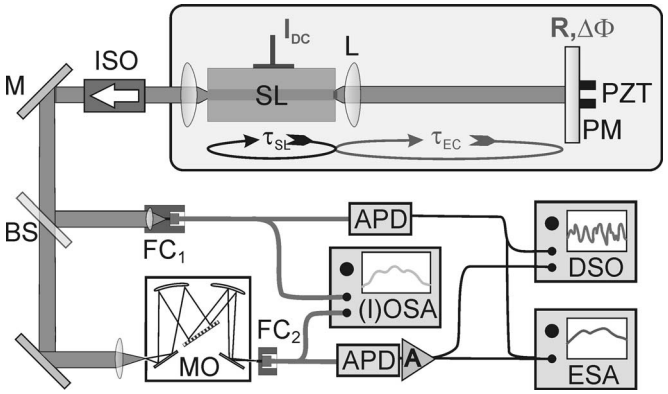

FIG. 1. Scheme of the experimental setup of the semiconductor laser feedback system.

Consequently, in Sec. V, we study this extraordinary broadband dynamics in detail in spectrally resolved measurements to gain deeper insight into the processes underlying the pronounced multimode emission. We discuss the spectral dynamics and motivate for the development of new models which can unveil the essential mechanisms determining the characteristic dynamics of this system. In Sec. VI, we summarize essential results and draw conclusions.

II. EXPERIMENTAL SETUP

In this section, we introduce the resonant short-cavities SL system and illustrate the experimental setup which we apply for analysis of the dynamical characteristics of the system. Figure 1 presents a schematic of the experimental setup. In the figure, the SL system is highlighted by a gray box which is located in the upper half of the figure, while the detection branch is mainly sketched in the lower half of the figure. The central device of the system is a ridge waveguide SL which emits at a center wavelength of 785 nm. The SL has been selected according to a small spectral spacing of the LMs and a broad, flat gain profile. The length of the semiconductor laser cavity is $L_{SL}=1.6$ mm and the effective refractive index of the gain material is $n=3.7$. Consequently, the longitudinal mode spacing corresponds to 25.3 GHz, which is also the round trip frequency of the light in the SL cavity $\nu_{SL}=25.3$ GHz. To guarantee well-defined operation conditions, the laser is pumped by an ultra-low-noise dc-current source and its temperature is set at 22.2 °C and stabilized to better than 0.01 K. The maximum output power of the SL is 109 mW at the upper limit of the pump current being $I_{DC}=150$ mA. For these conditions, the maximum relaxation oscillation frequency of the carriers-photon system, which represents a relevant frequency for the dynamics of the SL system, has been determined to be $\nu_{RO,max}=3.3$ GHz. Furthermore, we have measured the linewidth enhancement factor which expresses the strength of the nonlinearity in the SL to be $\alpha=2.0\pm0.2$. This has been done by applying the method proposed by Henning and Collins [32].

In the experiments, the light emitted from the front (right) facet of the SL is collimated by a lens (L) and propagates toward a partially transparent mirror (PM) with reflectivity

R. A part of the light is reflected from the PM and is reinjected into the SL after the delay time $\tau_{EC}=2L_{EC}/c$, and with the phase difference $\Delta\Phi=\Phi(t)-\Phi(t-\tau_{EC})$. Here, L_{EC} denotes the length of the external cavity, and c represents the speed of light in air. In the experiments, the ratio between L_{EC} and the optical length of the semiconductor laser cavity $L_{SL,opt}=nL_{SL}$ has been chosen between 2 and 5. This corresponds to external cavity round trip frequencies of 5.1 GHz $\leqslant \nu_{EC} \leqslant$ 12.7 GHz. For such short external cavity lengths, the short-cavity regime (SCR) requirement [13,17] is fulfilled, since the external cavity round trip frequency $1/\tau_{EC}$ is always sufficiently larger than $\nu_{RO,max}=3.3$ GHz. For these conditions, the key parameters of the system determining the dynamical behavior are the delay time τ_{EC}, the pump current I_{DC}, the feedback ratio γ, the feedback phase $\Delta\Phi$, and the ratio between the length of both cavities M. The feedback ratio γ describes the strength of the feedback and is defined as the ratio between the power of the light effectively coupled back into the SL and the power emitted at the front facet of the SL, $\gamma=P_{fb}/P_{out}$. The control parameters can be varied by changing L_{EC}, exchanging the PM by one with different reflectivity R, by varying I_{DC} and by shifting the PM on a subwavelength scale with a piezoelectric transducer (PZT). The light emitted from the rear facet of the SL is sent to the detection branch, which is isolated by an optical isolator (ISO) to shield the SL system from unwanted feedback from the detection branch. The light is divided at the nonpolarizing 50/50 beam splitter (BS). One part of the signal is coupled into a fiber at the fiber coupler (FC_1) and further subdivided for analysis of the emission properties. One fraction of the light is detected by a 12 GHz photodetector (APD), whose electric output is monitored on a digital storage oscilloscope (DSO) with an analog bandwidth of 4 GHz (at a sampling rate of 20×10^9 samples/s), and an rf spectrum analyzer (ESA) with 18 GHz bandwidth. The other fraction of the light can be either analyzed utilizing an optical grating spectrum analyzer with a resolution of 24 GHz (OSA) or by an interferometric spectrum analyzer (IOSA) with a resolution of up to 4 GHz. To gain insight into the properties of the dynamics generated in different optical spectral regions, the part of the light which propagates through the BS is coupled to a grating monochromator (MO) where it is spectrally filtered. The filtered light passing through the MO is coupled into a fiber at FC_2 for detection. The optical spectral bandwidth (3 dB) of the filtered light amounts to approximately 170 GHz, which is equivalent to an interval comprising seven LMs of the SL. The center wavelength of the spectral filter can be tuned over the entire emission spectrum of the SL system. In analogy to the detection of the total intensity dynamics, the detection apparatus for the spectrally filtered dynamics is identical, except for an additional rf amplifier (A) inserted after the APD accounting for the reduced intensity caused by spectral filtering and additional losses due to lower coupling efficiency at FC_2. In the following, we refer to the corresponding measurements as spectrally resolved measurements, since the spectral bandwidth of the filtered dynamics is sufficiently smaller than the maximum optical bandwidth of the total emission dynamics.

Before we experimentally investigate the characteristic dynamics of the SL system, we motivate for a particular choice of external cavity lengths. More precisely, we introduce resonant coupling between the semiconductor laser cavity and the external cavity so that the longitudinal modes (LMs) of the SL resonantly couple to the external cavity modes (ECMs). Our goal is to enhance the coupling between the LMs to achieve pronounced multimode dynamics comprising high optical bandwidth. Subsequently, we experimentally analyze the total intensity dynamics of the SL system in dependence on the pump current and the feedback phase $\Delta\Phi$.

III. RESONANT CAVITIES CONDITION

The coupling conditions between the semiconductor laser cavity and the external cavity are of crucial importance for the dynamics properties of multimode SLs with optical feedback. This is due to the fact that the coupling influences the interactions between the lasing modes which, in turn, determine the dynamics of the system. In similarity to compound cavity lasers [33,34], resonance conditions between the cavities in this double-cavity system represent distinguished coupling conditions. This is particularly the case when the lengths of the resonators are of comparable size. Since we are interested in pronounced multimode dynamics, we have experimentally studied the possibility of substantial enhancement of the coupling between adjacent LMs by realizing resonance conditions.

In the experiment, the SL operates at $I_{DC}=2.6I_{th,sol}$, well above the solitary laser threshold current $I_{th,sol}=45.72$ mA. It is convenient to express the pump level in terms of the pump parameter (p), which is defined by the ratio $p=I_{DC}/I_{th,sol}$. The SL is subject to moderate feedback with $\gamma=0.16$ inducing a threshold reduction of 6.9%. We adjust the ratio between the external cavity and the SL cavity $M=L_{EC}/L_{SL,opt}$ to $M\approx3$. Then, we slightly vary L_{EC} around the resonance condition and monitor the effect on the optical spectrum of the emission. The results are presented in Fig. 2. The optical spectrum for $M=3.15$ presented in Fig. 2(a) reveals several broad peaks. These peaks correspond to groups of LMs which meet the constructive interference condition between the emitted light and the feedback. The excited LMs within these groups are subject to feedback with similar $\Delta\Phi$, while the phase difference between these groups corresponds to multiples of 2π. When approaching the resonance condition, the phase variation over the spectral range which is induced by the detuning between the cavities becomes smaller. This crucially influences the spectral emission properties which can be deduced from comparison of Figs. 2(a) and 2(b). On the one hand, approaching the resonance condition, we find an increasing number of excited modes within each of the groups of LMs, manifesting in broader peaks. On the other hand, Fig. 2(b) reveals that the spacing between the groups of lasing LMs increases, because of the smaller detuning between the cavities. For the resonance condition set to $M\approx3.00$ and $\Delta\Phi$ adjusted for constructive interference condition, we are able to achieve conspicuous broadband emission comprising numerous lasing LMs, which is clearly demonstrated in Fig. 2(c). Indeed, the resonant coupling scheme turns out to be very efficient. Further tuning the cavity ratio to $M=2.97$, which is presented in Fig. 2(d), we detune away

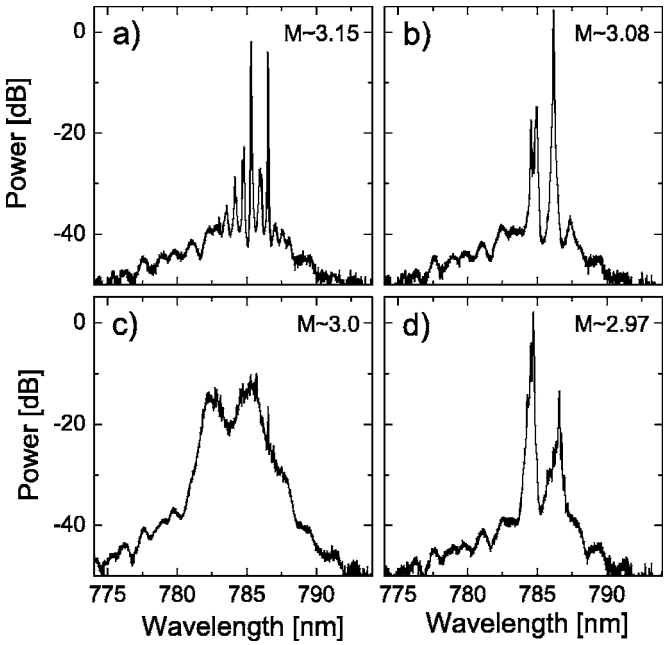

FIG. 2. Optical spectra for variation of L_{EC} around the resonance condition $M=3$. Longitudinal modes with similar $\Delta\Phi$ and which fulfill constructive interference conditions are excited. Approaching the resonance condition depicted in panel (c), more and more LMs strongly couple and are excited. In panel (a), the cavity ratio is $M\simeq 3.15$, in (b) $M\simeq 3.08$, in (c) $M\simeq 3.00$, and in (d) $M\simeq 2.97$, respectively. Other conditions are $\gamma=0.16$ and $p=2.6$.

from the resonance condition and observe similar but inverse behavior as for approaching the resonance condition. Hence, the best coupling conditions are accomplished when the round trip frequencies of both cavities, the semiconductor laser cavity ($\nu_{SL,opt}$) and the external cavity (ν_{EC}), fulfill an integer resonance condition $\nu_{SL,opt}/\nu_{EC}=M$, with $M=N$ being an integer number between 2 and 5. For this prerequisite, both resonators strongly couple and adjacent LMs are equally supported in the gain medium (semiconductor laser cavity) allowing for substantial coupling between LMs. Additionally, the feedback phase $\Delta\Phi$ is well defined in the SL system for integer resonance conditions, since each of the LMs is subject to feedback with the same value of $\Delta\Phi$. Depending on the gain profile, numerous LMs may be excited in the SL system offering potential for dynamics with considerable optical bandwidth.

Fractional ratios of $\nu_{SL,opt}/\nu_{EC}$, fulfill similar, although weaker, resonance conditions. In particular, half-integer resonance conditions sufficing $\nu_{SL,opt}/\nu_{EC}=M$ with $M=(2N+1)/2$ and N being an integer between 2 and 5 represent comparatively good coupling conditions. For half-integer resonance conditions, every next but one LM is subject to the same $\Delta\Phi$, while each of the LMs in between are subject to the π-shifted phase value $\Delta\Phi+\pi$. Accordingly, for $\Delta\Phi=N\pi$, one of these two groups of LMs is supported in the gain medium in a similar manner as for the integer resonance condition, while the LMs in between are considerably less supported. Therefore, in the case of half-integer resonance conditions, the mode spacing between every next but other mode is of importance for the emission properties. The corresponding frequency can be considered as a mode spacing frequency of a resonator of half the length of the original semiconductor laser cavity, $\nu'_{SL',opt}=2\nu_{SL,opt}$. For this frequency, in turn, an integer resonance condition is accomplished $M'=\nu'_{SL',opt}/\nu_{EC}$, with $M'=2N$. Intuitively, this situation differs from the original integer resonance condition only in the sense that the frequency spacing of supported modes is larger, which reduces the coupling strength between the supported modes. To verify these considerations, we perform experiments in which we vary M in the range between 2 and 5, while the other operation parameters are kept constant. In fact, for sufficiently strong feedback, we find similarly good coupling conditions for half-integer resonance conditions of $M=2.5$, 3.5, and 4.5 as for integer resonance conditions of $M=2$, 3, 4, and 5. This qualitative agreement is demonstrated in Fig. 3, in which we depict the corresponding optical spectra for $M=3$ in Fig. 3(a) and $M=2.5$ in Fig. 3(b). The figure discloses that for the integer and for the half-integer resonance condition, the LMs efficiently couple manifesting itself in pronounced optical broadband emission. In both cases, more than 130 LMs are lasing, spanning a spectral range exceeding 7 nm. The comparison with the optical spectrum for single-mode operation in the absence of optical feedback, which is represented by the gray line in Fig. 3(b), highlights the distinct multimode emission. In analogy to recent experiments on solitary multimode SLs which revealed dynamically induced switching between interacting LMs [35,36], the observed pronounced multimode emission properties immediately raises the question if the origin of the fascinating high optical bandwidth is of dynamical nature.

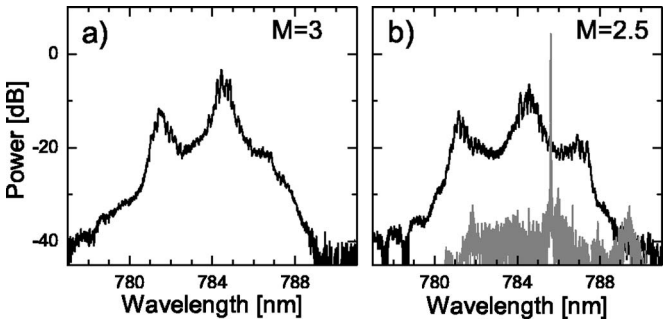

FIG. 3. Comparison of the spectral emission properties for integer cavity resonance condition $M=3$, depicted in panel (a), and half-integer resonance condition $M=2.5$, shown in panel (b). The feedback phase has been adjusted for maximum optical bandwidth. The feedback ratio amounts to $\gamma=0.16$ and pump parameter is $p=2.9$. The gray line in (b) depicts the optical spectrum of the solitary laser without optical feedback.

The anticipated answer is "yes." Accordingly, in Sec. IV, we analyze the dynamics of the SL system in detail and prove that for resonant coupling, we are able to achieve chaotic intensity dynamics with an extraordinarily high optical bandwidth of several nanometers. For the following experiments, we choose a ratio of $M=2.5$, since the larger spectral spacing of the supported modes facilitates better control over the dynamics. This property is especially helpful when studying the onset and the emergence of dynamics scenarios.

We point out that the results we obtain for the dynamics for $M=2.5$ agree to those for $M=3$, except for some quantitative differences with respect to the dependence on the control parameters.

IV. SCENARIOS OF THE DYNAMICS

In Sec. III, we have motivated our choice of the external cavity length being $L_{EC}=2.5L_{SL,opt}$. With this condition, we have met two distinct fundamental preconditions with respect to the dynamics of the system. First, the system fulfills the SCR requirement $\nu_{EC}/\nu_{RO}\gtrsim 1$ for the accessible range of parameters. Therefore, the resonant short-cavities SL system is still a delay system being mathematically infinite dimensional. This offers potential for generation of high-dimensional dynamics. Second, another fundamental precondition is realized by selection of comparable round trip times inside the short external cavity, $\tau_{EC}\approx 100$ ps, and in the semiconductor laser cavity, being $\tau_{SL}=2L_{SL,opt}/c\approx 40$ ps. For adjusted resonance conditions, this property allows for strong coupling of the LMs, because the LMs are only separated by very few (2–5) external cavity modes. Therefore, the fixed point structure of the system will be rather a global one and fundamentally different if compared to conventional multimode LK systems. In conventional LK systems, we typically find individual fixed point structures (LK ellipse) which are associated with the spectrally larger spaced LMs. Because of the wide spacing of the LM, the fixed point structures of adjacent LMs usually do not overlap. Hence, coupling between the LMs is not very strong in conventional LK systems.

In the following, we analyze the dynamics properties of the resonant short-cavities SL system and identify the pump current I_{DC} and the feedback phase $\Delta\Phi$ as major control parameters. Henceforth, we study their influence on the dynamical properties of the SL system.

A. Influence of the pump parameter

In this section, we investigate the dependence of the dynamics on the pump current. In the experiment, we set the feedback ratio to $\gamma=0.16$, inducing a threshold reduction of 6.9 %. For these conditions, we increase the pump parameter from $p=0$ to $p\approx 3$.

Starting at $p=0$, we find the onset of dynamics for $p=0.93$. For such small values of the pump parameter, the dynamics consists of slow intensity fluctuations comprising frequencies of up to several hundred MHz. However, the intensity fluctuations are not equally distributed, but cluster around a center frequency giving rise to a broad peak in the rf spectrum. The peak frequency increases as the pump parameter is increased. The peak frequency of the slow intensity fluctuation is not always present. Instead, we find a (cyclic) scenario for increasing pump parameter on a scale of $\Delta p\approx 0.14$. In this scenario, the dynamics evolves from stable emission to slow intensity fluctuations with a center frequency of a few hundred MHz, until the dynamics suddenly disappears and the emission becomes stable again. Nevertheless, the average peak frequency of the dynamics increases

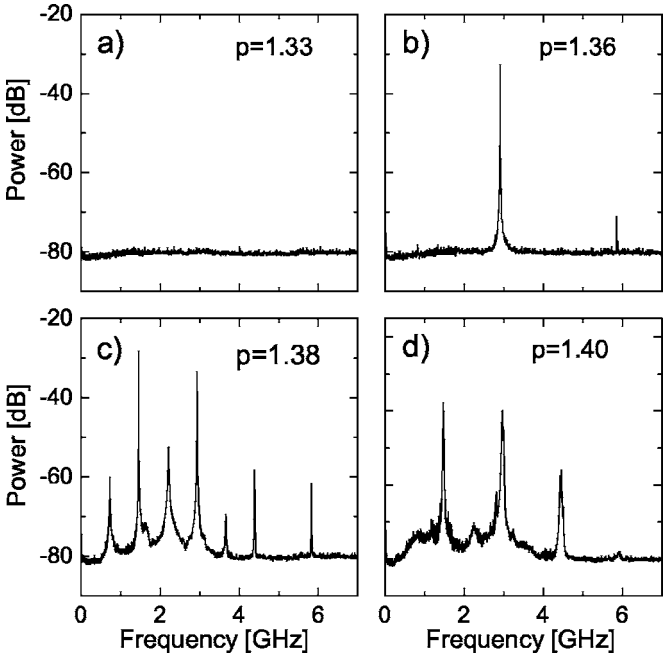

FIG. 4. The rf spectra of characteristic intensity dynamics of the cyclic scenario for intermediate pump levels. The dynamics evolve from stable emission in (a), to periodic states in (b) and (c), to chaotic dynamics (d), and then back to stable emission. The feedback ratio is moderate, $\gamma=0.16$, and the pump parameters are (a) $p=1.33$, (b) $p=1.36$, (c) $p=1.38$, and (d) $p=1.40$.

continuously for the incrementing pump current. For this feedback ratio, approximately two cycles of this scenario can be found until the dynamics change for pump levels of about $p=1.2$. At this level, an additional higher frequency component emerges at 2.7 GHz, which is not directly related to the relaxation oscillation frequency $\nu_{RO}\approx 0.6$ GHz. Further increasing the pump parameter, the low frequency dynamics becomes less and less pronounced, until it vanishes, while the new higher frequency component dominates the dynamics. Nevertheless, the property of the dynamics to evolve cyclically, mediating between stable emission and dynamics, not only persists, but becomes more and more pronounced.

An example of one cyclic scenario for intermediate pump parameters is presented in Fig. 4. Stable emission is achieved for a pump parameter of $p=1.33$, which is demonstrated by the corresponding flat rf spectrum depicted in Fig. 4(a). For slightly increasing the pump level, the intensity starts to oscillate periodically at a frequency of 2.91 GHz. This oscillation becomes more pronounced and slightly shifts to higher frequencies as p is increased to $p=1.36$. In the rf spectra in Fig. 4(b), we identify a peak corresponding to the periodic oscillation at its fundamental frequency at 2.92 GHz. Additionally, we find a weakly pronounced second harmonic at 5.84 GHz, while we do not find any dynamics directly related to the relaxation oscillations of the solitary laser, which have been determined to be $\nu_{RO}\approx 1.5$ GHz. We find that the fundamental period of the oscillation only slightly depends on p and γ, while it is independent of the choice of resonance condition and, in particular, it is not related to L_{EC}. This suggests that the oscillations are determined by the properties of the SL system. With further incrementing of the

pump parameter, we find indications of a period-doubling scenario, which becomes clear from the rf spectrum illustrated in Fig. 4(c) for which the pump parameter is $p=1.38$. For this pump level, we have already reached a period-4 state of the dynamics, via a period-2 region. In this case, we find an unusual pronounced first subharmonic of the fundamental frequency instead of the typical scaling behavior predicted by Feigenbaum [37]. This is probably due to resonance between the first subharmonic, located at 1.46 GHz, and the relaxation oscillations around 1.5 GHz. We note that for higher pump currents, for which ν_{RO} substantially increases, while the frequency of the first subharmonic only slightly increases, resonance is lost and the peak of the first subharmonic is less pronounced. In the experiments, we can identify period doubling up to the period-8 region, giving strong experimental evidence for an actual period-doubling cascade. Due to the period doubling, we expect chaotic dynamics for higher pump parameters. Indeed, chaotic dynamics can be achieved for $p=1.4$, which is demonstrated by the rf spectrum given in Fig. 4(d). The figure discloses that the peaks related to the originally periodic dynamics are significantly broadened. Now, the rf spectrum reveals an enhanced bandwidth of the dynamics of ~5 GHz reflecting chaotic dynamics. We point out that at the onset of chaos, the optical spectrum does not give evidence for multimode dynamics. In that sense, the dynamics becomes locally chaotic at the onset of chaos. An additional interesting characteristic of the period-doubling route to chaos can be identified from the rf spectrum illustrated in Fig. 4(d). For increasing the pump parameter and progressing into the chaotic regime, we can identify the inverse cascade. In particular, the residuals of the period-4 peaks are considerably suppressed in Fig. 4(d). Finally, the cycle is complete, the chaotic dynamics suddenly disappear, and the steady emission state is reached again. This transition between the chaotic and the steady state exhibits hysteresis when decreasing the pump parameter.

The corresponding optical spectra for intermediate pump parameters reveal that with increasing the pump parameter, the chaotic dynamics also comprise a growing number of LMs extending the optical bandwidth. Therefore, we have substantially increased the pump parameter to verify if the SL system allows for generation of pronounced chaotic intensity dynamics in conjunction with multimode emission comprising high optical bandwidth. In the experiment, we adjust the pump parameter to $p=3.28$, for which we find pronounced chaotic dynamics. The results are summarized in Fig. 5. The black line in Fig. 5(a) depicts the rf spectrum of the dynamics. The continuous spectrum reveals pronounced chaotic intensity dynamics with a bandwidth of exceeding 6 GHz. Furthermore, the spectrum does not disclose obvious remnants of periodic frequencies from the period-doubling scenario as in the case of lower pump levels in Fig. 4(d). Now, the transition from stable to chaotic dynamics takes place in a very small interval, which is in contrast to the noticeable period-doubling cascade observed for small pump parameters. However, we can identify two specific regions in the rf spectrum. First, there is a broad peak at around 1.3 GHz, which cannot be directly associated with a characteristic system frequency. Second, a very broad hump can be identified with a maximum at 3.2 GHz which might be related to the relaxation oscillations, being $\nu_{RO}=3.06$ GHz for this pump parameter. A 20 ns long segment of the time series is provided in Fig. 5(b), which illustrates the irregular intensity fluctuations on subnanosecond time scale. The corresponding optical spectrum is presented in Fig. 5(c). In contrast to the behavior for small p, the optical spectrum for chaotic dynamics achieved for high p reveals an extraordinarily high spectral bandwidth of about 7 nm. Since the spacing of the LMs amounts to 52 pm, the number of modes involved in the dynamics exceeds 130. An interesting feature of the broadband optical spectrum is its tridentlike envelope. We have experimentally verified that this effect does not originate from detuning of the external cavity or dispersion effects in the SL material. This property seems to be a general property for our multimode system. The underlying mechanisms leading to this structure are currently investigated. Furthermore, we note that only for resonant coupling conditions, we are able to achieve such intriguing optical broadband emission. To highlight the dramatic increase in the optical bandwidth, in Fig. 5(d), we present an optical spectrum for stable emission achieved for small decrementing of the pump level by $\Delta p=-0.03$ to $p=3.25$. This gives also evidence that the cyclic dependence of the dynamics for increasing (and decreasing) pump parameter persists for high pump levels. For completeness, we depict the flat rf spectrum corresponding to stable emission as gray line in Fig. 5(a). Comparison of both rf spectra reveals that the low frequency

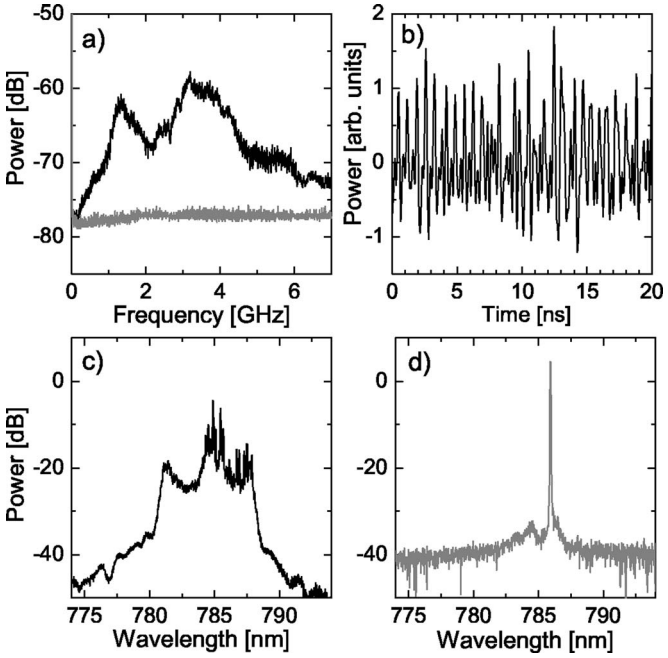

FIG. 5. Dynamics observed for high pump parameter $p=3.28$ and moderate feedback ratio $\gamma=0.16$. The rf spectrum of the dynamics, represented by the black line in panel (a), reveals broadband chaotic dynamics. Panel (b) shows a segment of the corresponding time series, while panel (c) demonstrates pronounced multimode emission manifesting in the broadband optical spectrum. For comparison, panel (d) depicts the optical spectrum for single-mode emission, which is obtained for a slight change of p to $p=3.25$. The corresponding rf spectrum is represented by the gray line in panel (a).

part of the rf spectrum for chaotic emission is at the detection noise floor. This indicates that the average power of the SL light source for optical broadband emission is constant, or more precisely, it exhibits low relative intensity noise (RIN) with respect to relevant time scales for technical applications.

At first glance, the origin of the observed cyclic character of the scenario for linearly changing p might be surprising. However, a simple explanation can be given by the indirect influence of the pump parameter on the feedback condition. For increasing the pump parameter, the cavity length of the semiconductor laser $L_{SL,opt}$ slightly elongates because of thermal effects. This causes a small redshift of the emission wavelength inducing a small decrease of $\Delta\Phi$, which is a cyclic parameter.

B. Influence of the feedback phase

In this section, we verify whether the feedback phase is the relevant parameter determining the cyclic nature of the observed scenario. Therefore, we study the effect of small changes of $\Delta\Phi$ on the dynamics. Experimentally, a phase shift can be induced via a small variation of L_{EC} on a subwavelength scale which can be realized by application of the piezoelectric transducer (PZT), illustrated in Fig. 1. For proper calibration of the phase parameter $\Delta\Phi$, we have measured the change of L_{EC} in dependence on the voltage supplied to the PZT using a high-resolution range meter. We find that a change of 5.5 V induces a variation of $\Delta L_{EC}=\lambda/2$ which shifts $\Delta\Phi$ by 2π. We note that for resonant coupling conditions, a proper feedback phase $\Delta\Phi$ is defined, as we have discussed in Sec. III. The resonance condition implements the same $\Delta\Phi$ for all LMs under the premise that dispersion in the SL medium is negligible. This is the case for the presented system for which we have measured a maximum dispersion-induced deviation from $\Delta\Phi$ of only $\pm 4\%$ within the entire optical spectrum.

Figure 6 depicts rf spectra of the intensity dynamics for different values of the feedback phase $\Delta\Phi$. In the experiment, we chose operation conditions for fully developed chaotic dynamics. Accordingly, we apply moderate feedback of $\gamma=0.16$ and adjust for high pumping of $p=3.28$ for which we measure the relaxation oscillation frequency to be $\nu_{RO}=2.5$ GHz. First, we adjust $\Delta\Phi$ for continuous emission by controlling the voltage supplied to the PZT. The corresponding rf spectrum is presented in Fig. 6(a) and does not reveal indications of dynamics. Since this condition can be easily recognized, we have chosen it as reference and associate it with $\Delta\Phi=0$. For decreasing the feedback phase from this condition, we find a very similar cyclic scenario as for continuously increasing p. To determine its periodicity, we measure the corresponding phase difference for a cycle of the scenario and find π periodicity. In the following, we illustrate the emergence of chaotic dynamics within one cycle of the dynamics.

The stable emission state depicted in Fig. 6(a) is the starting point. From this state, we decrease $\Delta\Phi$ and monitor the influence in the rf spectrum of the dynamics. For $\Delta\Phi \approx -0.2\pi$, we find the onset of periodic dynamics. Then, in

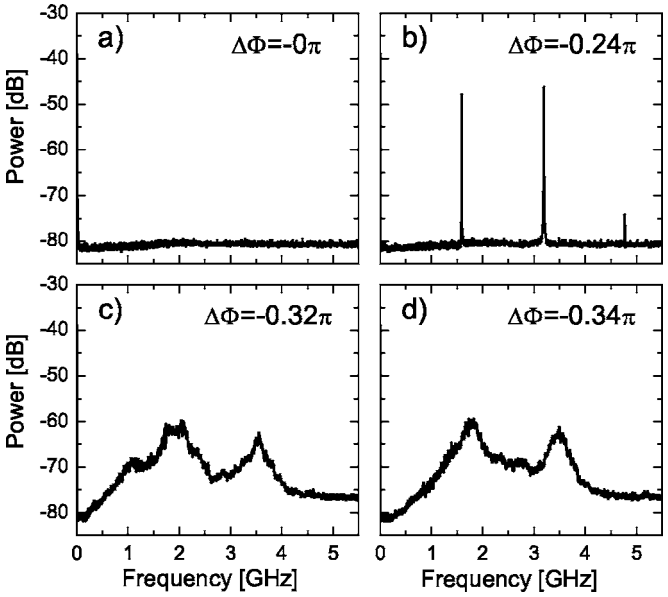

FIG. 6. The rf spectra of characteristic dynamics of the π-cyclic scenario for decreasing feedback phase $\Delta\Phi$. The phase condition for stable emission, illustrated in panel (a), has been assigned to the phase value $\Delta\Phi=0\ \pi$. Period-2 dynamics for $\Delta\Phi=-0.24\ \pi$, which emerged from period doubling, is presented in panel (b). Onset of chaos is obtained for $\Delta\Phi=-0.32\ \pi$, depicted in panel (c). While fully developed chaotic dynamics is achieved for $\Delta\Phi=-0.34\pi$, shown in panel (d). Other conditions are $p=3.3$ and $\gamma=0.16$.

agreement with the observations for increasing p, a period-doubling scenario evolves with the period-2 state for $\Delta\Phi=-0.24\pi$, illustrated in Fig. 6(b). For further decreasing $\Delta\Phi$, we find the period-4 state and subsequently a quick transition to chaos around $\Delta\Phi=-0.28\pi$. The observed development of the dynamics qualitatively agrees to the period-doubling behavior we have discussed in Sec. IV A for Fig. 4. However, we note that for this high level of pumping, the route to chaos takes place within a very small range of the control parameter between $-0.20\pi<\Delta\Phi<-0.28\pi$. For further decreasing $\Delta\Phi$, the dynamics evolve within the chaotic regime. This becomes clear from the broad and continuous rf spectrum for $\Delta\Phi=-0.32\pi$ depicted in Fig. 6(c). Nevertheless, even within the chaotic regime, the dynamics develop, which is indicated by slight differences in the rf spectra. Figure 6(d) presents the rf spectrum of chaotic dynamics for $\Delta\Phi=-0.34\pi$, which is close to the sudden transition back to stable emission observed for $\Delta\Phi=-0.36\pi$. Approximately 10 indistinguishable cycles of this scenario can be identified for changing the voltage supplied to the PZT. We have also investigated scenarios of the dynamics for different pump parameters and found very good agreement between the dynamics observed for variations of $\Delta\Phi$ and that for changing p. It is worth noting that in all of the experiments, we do not find indications of intensity dynamics related to the external cavity round trip frequency $\nu_{EC}=10.1$ GHz. Although the corresponding frequency lies within the detection bandwidth, we find an absence of dynamics related to ν_{EC} for different integer and half-integer resonance conditions of up to $M=5$. This remarkable property might originate from the comparatively slow relaxation oscillations of the SL ($\nu_{RO,max}$

=3.3 GHz), which determine the maximum bandwidth of the dynamics.

The sensitive dependence of the dynamics on variations of $\Delta\Phi$ and the cyclic nature of the dynamics suggests similarity to the short-cavities regime (SCR) dynamics of nonresonant LK SL systems [13,38]. However, in contrast to this similarity, we find distinct differences between the conventional SCR regime dynamics and the dynamics of the resonant short-cavities SL system. First, we have identified a period-doubling route to chaos instead of the quasiperiodic route that is characteristic for SCR dynamics. We note that Ryan *et al.* gave numerical evidence for period doubling for a multimode (five LMs) nonresonant short-cavities LK SL system [17]. However, period doubling has been only identified for weak feedback, which is in contrast to our observations. Second, we have experimentally demonstrated π periodicity instead of the characteristic 2π periodicity for SCR dynamics. Since this result is quite surprising, we have analyzed the modal structure of the compound cavity system for different resonance conditions and in dependence on $\Delta\Phi$. We find that in the case of half-integer resonance conditions, the modal structure for $\Delta\Phi$ is identical to that of $\Delta\Phi' = \Delta\Phi + \pi$, but shifted by $\Delta\nu_{LM}$. Therefore, a phase shift of $\Delta\Phi$ only leads to a change in the dominant group of LMs, as we have discussed in Sec. III. For the integer resonance conditions, on the other hand, an identical modal structure is only expected for a phase shift of 2π. In contrast to this, in the experiments, we find similar dynamics for the cycle between $0\pi \leqslant \Delta\Phi < \pi$ and $\pi \leqslant \Delta\Phi < 2\pi$. In this case, a closer look at the modal conditions for integer resonance conditions $M \geqslant 2$ indicates similarities for the supported modes and their neighbors for $\Delta\Phi' = \Delta\Phi + \pi$. This similarity might be the origin of this appearing π periodicity. We note that at the present time, the details about the occurrence of this π-periodic similarity of the dynamics for integer resonance conditions are not fully understood. Insight into this interesting problem could be gained from analysis of appropriate models which also consider the dynamics properties of the SL system. Nevertheless, in both cases, the cyclic dependence of the dynamics on the control parameters can be attributed to the cyclic nature of $\Delta\Phi$. Third, the dynamics do not reveal components related to the external cavity round trip frequency ν_{EC} which plays a key role for conventional SCR dynamics. Finally, the most conspicuous difference between the dynamics of both systems consists in the distinct optical broadband emission, comprising more than 100 LMs, which is unique for the presented system. The emergence of this intriguing property and its relation to the intensity dynamics deserves detailed investigation.

C. Optical spectral properties

It is well known that the occurrence of feedback-induced intensity dynamics for conventional LK systems is linked to the emergence of spectral dynamics, which is due to the α parameter. This results in an enhancement of the linewidth. For this reason, this phenomenon has been termed coherence collapse [15]. However, although this phenomena is well known, detailed studies on the influence of the dynamics on the coherence properties of SLs with optical feedback are rare and the reported studies focus on conventional operation conditions [39,40]. However, in analogy to conventional SL systems, we can also expect spectral dynamics in conjunction with intensity dynamics for our resonant short-cavities system. In the following, we investigate this in detail and study potential interrelations between the intensity dynamics and the spectral properties.

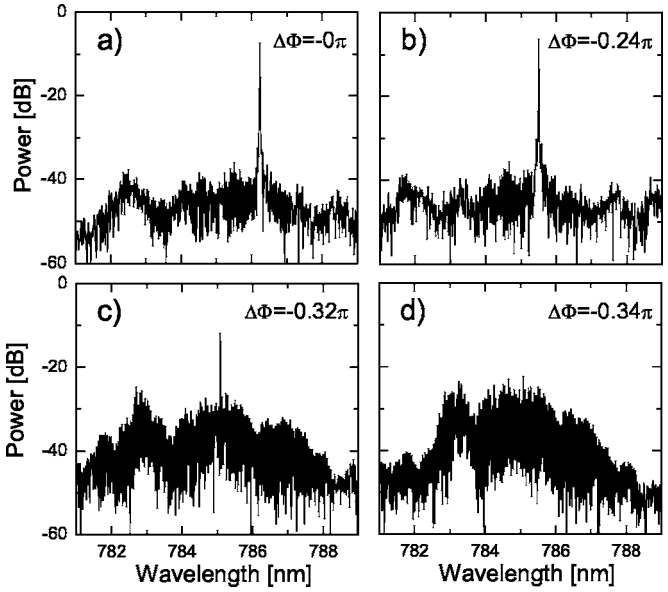

FIG. 7. Optical spectra corresponding to the characteristic dynamics scenario presented in Fig. 6. The parameters are specified in the captions of Fig. 6.

Therefore, we have simultaneously recorded the optical spectra and the intensity dynamics. This allows for direct comparison of both characteristics. Figure 7 presents the optical spectra corresponding to the rf spectra of the intensity dynamics of Fig. 6. The optical spectra have been recorded with a high-resolution interferometric optical spectrum analyzer (IOSA) with a resolution of 4 GHz. This resolution is sufficient to fully resolve the LMs and the external cavity modes with a spacing of $\Delta\nu_{LM}$=25.3 GHz and $\Delta\nu_{EC}$ =10.1 GHz. Since the IOSA is based on a Michelson interferometer, it allows in addition for direct measurement of the visibility functions, which are depicted in Fig. 8. This is beneficial, since this provides direct insight into the coherence properties of the SL system.

By analogy to Fig. 6(a), we start the analysis of the spectral properties for stable emission at $\Delta\Phi=0\ \pi$. The resulting optical spectrum is presented in Fig. 7(a). The spectrum exhibits single-mode emission with a side-mode suppression exceeding 30 dB. Figure 8(a) shows the corresponding visibility function. The visibility function is almost constant around maximum visibility and does not give evidence for decreases within the accessible range. Hence, the coherence length (L_{coh}) of the emitted light is beyond the resolution of the IOSA. Nevertheless, for stable single-mode emission, we can determine L_{coh} by measuring the linewidth with a Fabry-Perot scanning interferometer. The result gives L_{coh}=7.8 m, which is somewhat longer than the coherence length of the solitary laser for the same operation conditions $L_{coh,sol}$

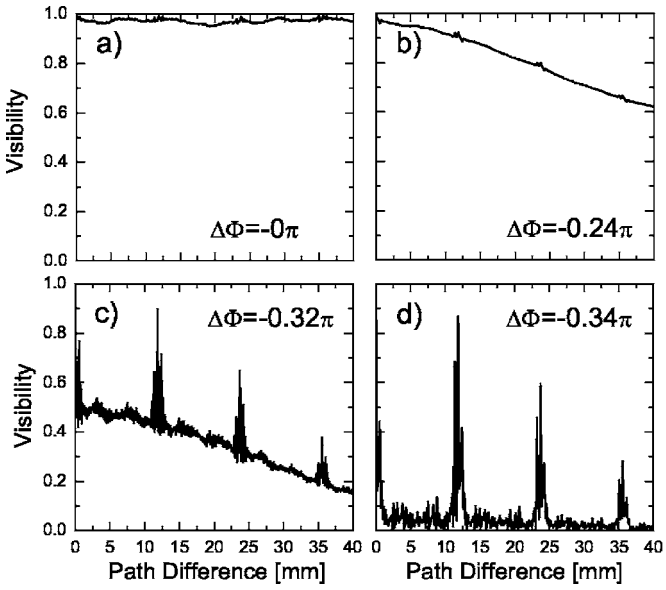

FIG. 8. Visibility functions corresponding to the dynamics and the optical spectra depicted in Figs. 6 and 7, respectively.

=5.8 m. However, the spectral properties appreciably alter for tuning $\Delta\Phi$ away from the stable emission state when entering the regime of dynamics. Figure 7(b) presents the optical spectrum for the period-2 state for $\Delta\Phi=-0.24\pi$, slightly beyond the onset of dynamics. Interestingly, the optical spectrum remains single mode, but with slightly broadened linewidth. This results in considerable reduction of the coherence length, as it can be seen in Fig. 8(b). In this case, the coherence length can be extrapolated to $L_{coh}\approx 0.7$ m. Further decreasing $\Delta\Phi$ within the regime of periodic intensity dynamics continuously enhances the linewidth and reduces the coherence length. We note that for periodic dynamics, we find hints for very weakly pronounced external cavity side modes near the central LM. At the onset of chaos for $\Delta\Phi=-0.32\ \pi$, we find reduced intensity for the dominant LM, but also numerous LM side modes that are suddenly involved in the dynamics. This feature is illustrated in Fig. 7(c) in which we identify that the intensity of the LMs in the range between 781.8 nm and 788.2 nm has considerably increased. At first sight, the optical spectrum might look noisy, but we emphasize that this is not the case. The spectrum is very stable, while its noisy appearance is due to the high resolution of the IOSA revealing more than 120 LMs participating in the emission. This sudden coupling of the LMs drastically affects the coherence properties, which is depicted in Fig. 8(c). The visibility function discloses peaks at multiples of 11.9 mm. This path difference equals twice the optical length of $L_{SL,opt}$. The envelope of the peaks describes a curve with similar shape as the one presented in Fig. 8(b), but with faster falloff. Additionally, Fig. 8(c) reveals a drastic decay of the visibility within 1 mm down to ≈ 0.5. Between the peaks, the visibility continuously decreases for increasing path difference. This sudden reduction of the visibility occurs as soon as the LMs couple, inflating the spectral bandwidth. Further increasing the feedback phase to $\Delta\Phi=-0.34\pi$, the intensity dynamics in Fig. 6(d) reveals fully developed chaos. The corresponding optical spectrum is depicted in Fig. 7(d). The spectrum reveals pronounced multimode emission comprising about 100 LMs in a spectral range of ~ 5 nm, which suggests further reduction of the coherence. Indeed, the visibility function in Fig. 8(d) exhibits fast falloff of the visibility below $1/e$ within only 130 μm. For a larger path difference, the visibility rapidly drops to almost zero. Only the peaks related to the length of the semiconductor laser cavity located at multiples of $2L_{SL,opt}$ exhibit considerable visibility. However, the envelope of the peaks also gives rise to a slightly faster falloff, if compared to that of Fig. 8(c). We note that these remnants of visibility can be reduced by increasing the dynamical bandwidth of the SL system. Since the corresponding peaks in the visibility are related to the spacing of the LMs, this property of the visibility function already indicates correlations between adjacent LMs, which can be influenced by modification of the coupling conditions between the LMs. We will study the interactions between the LMs in Sec. V.

The presented results are interesting from both the fundamental NLD-oriented and the application-oriented point of view. The experiments have revealed a strong interrelation between the intensity dynamics and the spectral dynamics. Interestingly, the dynamics emerge in a spectrally well-confined region in vicinity of the lasing LM. In this regime, the dynamics only enhances the linewidth of the central LM which, in turn, reduces the coherence length. At the onset of chaos, the spectral dynamics in the vicinity of the central LM suddenly starts to inflate because of coupling of numerous LMs. For fully developed chaos, the LMs strongly couple and multiple LMs participate in the dynamics, giving rise to rather global dynamical behavior. The onset of this characteristic multimode emission is fascinating since it might reveal general properties of pronounced multimode dynamics which have also been reported for other laser systems, such as for fiber lasers [41]. Intuitively, the pronounced multimode emission can result from spectral overlap of the dynamics of adjacent LMs. Since for resonant feedback $\Delta\Phi$ is similar for all the LMs, the relative spectral position between the external cavity modes and the LMs is similar for all LMs. This means that once the central LM couples to its neighboring LMs, these LMs also couple to their neighbors and so forth. However, further investigations are necessary to fully understand the underlying mechanisms. Such understanding is also required for optimization of the emission qualities with respect to technical applications.

We have demonstrated that the coherence properties of this system can be efficiently controlled and varied in a wide range between approximately 130 μm and 8 m by application of NLD. In particular, low-coherent light sources have recently attracted much attention, since they are required for realization of modern measurement technology such as chaotic light detection and ranging (CLIDAR) [7] and coherence tomography [42]. The resonant short-cavities SL system offers excellent qualities for implementation of such technology, since it allows for the rapidly decaying visibility function within the range of ~ 130 μm. Although the applied principle for reduction of the coherence length is based on chaotic emission dynamics, the average output power of the light source is constant on the technically relevant time scales. This can be deduced from Fig. 5(a). Furthermore, the

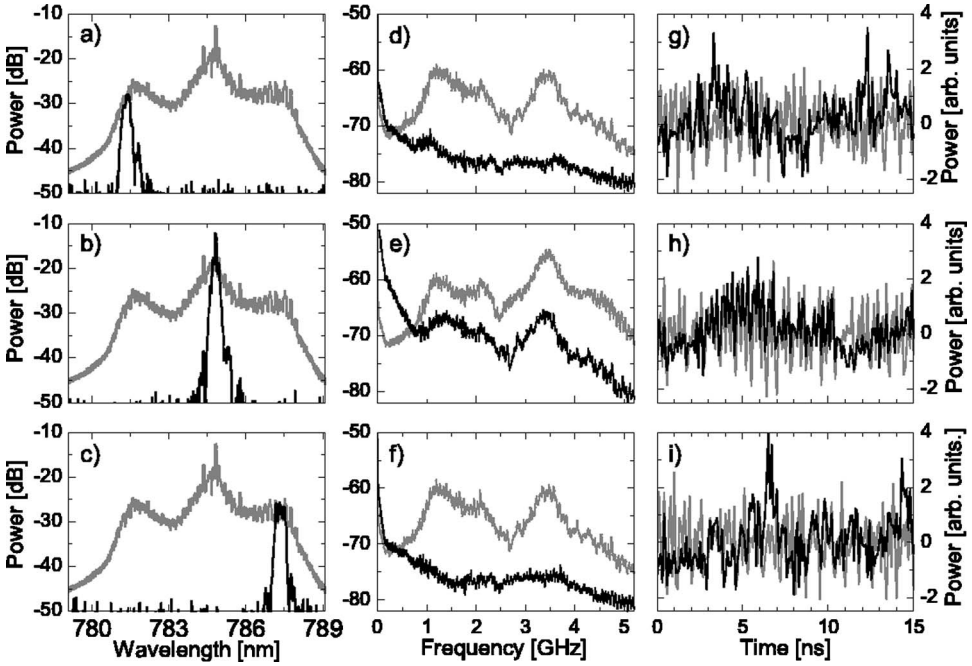

FIG. 9. Comparison of total and spectrally filtered dynamics for optical broadband emission. The three different center frequencies of the filter correspond to 781.7 nm in (a), 784.8 nm in (b), and 787.3 nm in (c). The total dynamics are represented in gray and the filtered dynamics in black. The optical spectra are depicted in (a), (b), and (c), while the corresponding rf spectra and the normalized time series are presented in (d)–(f) and (g)–(i), respectively. Other parameters are $p=2.52$ and $\gamma=0.18$.

light source exhibits the good beam properties of a laser and offers a maximum output power of 100 mW. We note that there are also recurrent regions of higher visibility at multiples of $2L_{SL,opt}$. For high-resolution ranging, the fast falloff of the visibility is relevant with a corresponding coherence length of ~ 130 μm. Nevertheless, other applications might exist for which the visibility peaks may become of importance. From the NLD point of view, in turn, the recurrent peaks of the visibility are very fascinating. The fact that the spacing of the peaks $\Delta L_{peak}=2L_{Sl,opt}$ is related to the spacing of the LMs $\Delta\nu_{LM}=c/\Delta L_{peak}$ already suggests that the dynamics of the LMs is correlated. This observation raises the question of possible interactions between the LMs and their role for the occurrence of pronounced multimode emission.

V. INTERACTIONS OF THE LONGITUDINAL MODES

In this section, we study interactions between the LMs for the optical broadband dynamics. Therefore, we perform spectrally resolved measurements, similar to the techniques presented in Refs. [35,36,43]. In the experiment, we simultaneously acquire the total intensity dynamics, comprising all the LMs, and spectrally filtered dynamics, comprising the dynamics of only seven LMs. Then, we compare both dynamics and repeat the procedure for different filter positions. From this, we gain insight into the role of the particular spectral components to the total intensity dynamics. In the experiment, we realize spectral filtering using the grating monochromator (MO) illustrated in Fig. 1. We chose similar conditions as for the previous experiments: moderate feedback of $\gamma=0.18$ and moderate, but slightly reduced, pumping of $p=2.52$. Additionally, we adjust $\Delta\Phi$ for maximum optical bandwidth.

Figure 9 summarizes the results of the experiment. In the figure, the total dynamics is presented in gray, while the spectrally filtered dynamics is represented in black. To provide a complementary overview over the dynamics, we present the optical spectra, the rf spectra, and 15 ns long normalized time series of the intensity dynamics for measurements with three different filter positions. Each of the horizontal rows in Fig. 9 represents the results for one of the three filter positions which are 781.7 nm, 784.8 nm, and 787.3 nm. The optical spectra are depicted in the Figs. 9(a), 9(b), and 9(c) and exhibit an optical bandwidth of approximately 7 nm for the total dynamics. The 3 dB bandwidth of the filtered dynamics has been determined to be 350 pm. Accordingly, the spectrally filtered dynamics reflect the dynamics of seven LMs.

We start with the comparison of the total dynamics and the filtered dynamics in the vicinity of the center wavelength of the optical spectrum at 784.8 nm [Figs. 9(b), 9(e), and 9(h)]. The rf spectrum of the filtered dynamics in Fig. 9(e) reveals conspicuous dynamics for frequencies below 1 GHz which are lacking in the rf spectrum of the total dynamics. Besides this, both rf spectra show good qualitative agreement for the fast components of the dynamics between 2 GHz and 5 GHz. These two characteristics can also be identified by comparison of the corresponding time series which are presented in Fig. 9(h). On the one hand, the time series for the filtered dynamics exhibits slow intensity fluctuations on a time scale of several nanoseconds. Such slow fluctuations are absent in the time series of the total dynamics, giving evidence for antiphase dynamics of the LMs [44]. This phenomenon is well known for less pronounced multimode SL systems [45–48]. In many of these systems, competition of the LMs for the common gain has been identified as the origin of antiphase dynamics, since it induces considerable coupling between the LMs [24]. In contrast to the antiphase dynamics at low frequencies, we find in-phase dynamics in the time series for the fast pulsations on subnanosecond time scale. Such in-phase dynamics has also been reported for weakly pronounced multimode SL systems. For these systems, it has turned out that in-phase dynamics was related to the relax-

ation oscillations [46]. However, for the chosen operation conditions, the relaxation oscillation frequency amounts to $\nu_{RO}=2.6$ GHz, which substantially differs from the dominant peak at 3.5 GHz in the rf spectra. This different peak frequency can arise from feedback and multimode effects which influence the in-phase dynamics in this frequency range. Further insight into the interactions of the LMs is required for clarification of this problem. Therefore, we study the dynamics properties of spectral regions which are apart from the center of the optical spectrum. In the corresponding experiments, first, we decrease the center frequency of the filtered dynamics to 781.7 nm. Then, we increase the center frequency of the filter to 787.3 nm. The results are presented in Fig. 9 in (a), (d), and (g) and in (c), (f), and (i), respectively. The rf spectra are presented in Figs. 9(d) and 9(f). Both spectra of the filtered dynamics reveal more pronounced low frequency dynamics than the total intensity dynamics. This agrees with our previous finding for the filtered dynamics near the center of the optical spectrum presented in Fig. 9(e). In contrast to the dynamics near the center, the dynamics at the flanks of the optical spectrum evidence substantially less pronounced high frequency dynamics. This property is also reflected by the corresponding normalized time series, which are depicted in the Figs. 9(g) and 9(i). In both cases, the time series of the filtered dynamics exhibit low frequency intensity dynamics. In contrast to the intensity dropouts on slow time scales which can be recognized in Fig. 9(h), the slow dynamics for the spectrally distant regions consist of short intervals of increased power. The fast intensity pulsations, on the other hand, are considerably less pronounced. Furthermore, we do not find indications of distinct in-phase dynamics in time series of the spectrally distant regions.

The results indicate that mode competition is also a relevant mechanism for the resonant short-cavities SL system. Even more, we find evidence for considerable interactions of the LMs within the complete spectral range. On the contrary, the experiment discloses that the dynamics on the fast time scales beyond 1 GHz originates more from emission near the center of the optical spectrum. These results immediately raise the question, whether the dynamics is inherently broadband for all LMs disregarding the spectral position, or if the dynamics in the center drives the dynamics in spectrally distant regions. In terms of information-theory-based NLD, this question is directly related to the question about the generation and the flow of information. The answer to this problem provides fundamental insight into the modal interplay in pronounced multimode systems [49].

First access to this problem can be obtained from correlation analysis of the recorded time series. Figures 10(g), 10(h), and 10(i) present the calculated cross-correlation functions (Σ_{corr}) between the time series of the total intensity dynamics and that of the spectrally filtered intensity dynamics shown in Figs. 9(g), 9(h), and 9(i). In this representation, high correlation at negative times means that the spectrally filtered dynamics lags with respect to the total intensity dynamics. The cross correlation for the total intensity dynamics and the spectrally filtered dynamics of the central region is presented in Fig. 10(g). Σ_{corr} exhibits two features. First, it reveals a substructure which can be assigned to the fast dynamics with a dominant component around 3.5 GHz, as it

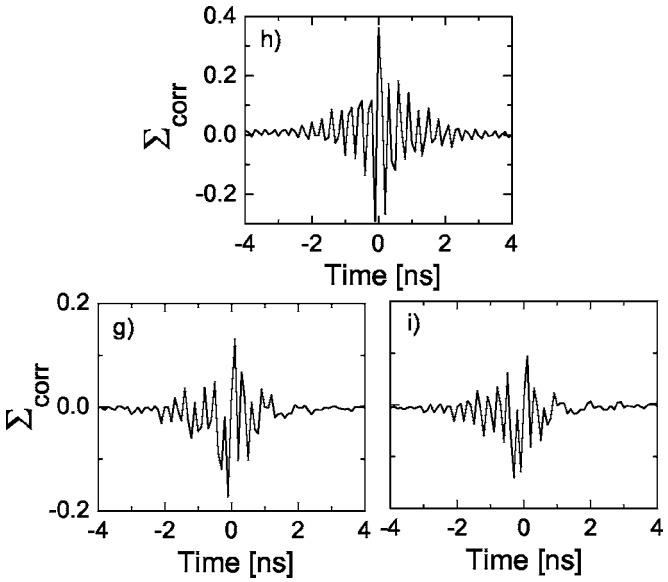

FIG. 10. Correlation functions between the total intensity and the spectrally filtered time series of the measurement presented in Figs. 9(g), 9(h), and 9(i). The center frequencies of the filter are 781.7 nm in (g), 784.8 nm in (h), and 787.3 nm in (i).

can be seen in Fig. 9(e). Second, we identify a far reaching envelope, which also gives rise to correlation between slower dynamics components. In this case, we find an almost symmetric envelope of the cross-correlation function and maximum correlation at zero lag. These properties indicate that the dynamics in the central region is simultaneously generated on both the slow and the fast time scales, if compared to the total intensity dynamics.

The correlation behavior changes for the spectrally distant regions as depicted in Figs. 9(g) and 9(i). In similarity to the central spectral region, for both cases, we find coinciding maximum cross correlation at zero lag. This discloses that the fast dynamics are also generated simultaneously with the fast dynamics generated near the central spectral region. The envelope of the cross-correlation function, on the other hand, reveals an asymmetric envelope with long-range, dominantly negative correlations for negative delays. This property can be attributed to comparably slow antiphase dynamics which lag with respect to the total intensity dynamics. Further experiments are required to gain deeper insight into the fundamental properties of the multimode interactions. In particular, cross-correlation measurements between fully resolved dynamics of spectrally distant regions can provide important information about the mechanisms underlying the pronounced multimode dynamics. These measurements are experimentally demanding and are subject to current investigations. Additionally, analysis of suitable models is a desirable, complementary approach to achieve this goal. Nevertheless, a suitable simple model, comparable to LK-based modeling, which is capable to account for the relevant resonant coupling condition is currently not available.

VI. CONCLUSIONS

We have presented detailed studies on the emission properties of a resonant short-cavities SL system with comparable

lengths of the external cavity and the semiconductor laser cavity. We have demonstrated that resonant coupling between both cavities efficiently enhances coupling between the LMs allowing for pronounced multimode emission. For resonant coupling, we have identified the feedback phase $\Delta\Phi$ as being a major control parameter determining the dynamics of the SL system. For continuously decreasing $\Delta\Phi$, the intensity dynamics evolve in a π-cyclic scenario from stable emission to periodic states, to chaos, and again back to stable emission. Analysis of the resonant short-cavities dynamics revealed conspicuous differences if compared to the well-known short-cavities regime dynamics exhibited by nonresonant SL systems [13,38]. A remarkable property of the presented system consists in the possibility of generating broadband chaotic intensity dynamics in conjunction with distinct multimode dynamics comprising an optical bandwidth of $\sim$7 nm. For this state, more than 130 LMs participate in the dynamics. Detailed analysis of the spectral properties of the dynamics revealed strong interrelations between the intensity dynamics and the spectral emission properties of the system. We have demonstrated that this property can be utilized for controlled adjustment of the coherence properties of the light, which offers an accessible range of coherence length between $\sim$130 μm and $\sim$8 m. In that sense, we have demonstrated that NLD can be beneficially harnessed for realization of light sources with customized emission properties. With respect to technical applications and from the fundamental point of view, understanding of the underlying mechanisms leading to the emergence of such extraordinarily pronounced multimode dynamics is desired. Consequently, we have performed spectrally resolved measurements of the dynamics that provided first insight into the complex dynamics. The results revealed considerable interactions between the LMs manifesting themselves in antiphase dynamics on time scales slower than nanoseconds. This result has been verified by detailed cross-correlation analysis, which has also given evidence that the fast components of the dynamics are simultaneously generated within the total spectral range.

From the NLD point of view, identification of the underlying mechanisms leading to such pronounced multimode dynamics is desired, since it might reveal general properties of complex multimode systems. Complete understanding of the dynamics requires further experiments such as fully spectrally resolved measurements allowing for analysis of inter-LM correlations. Such experiments are challenging and impose high demands on the measurement technology. Therefore, practical models are desired which can provide complementary insight. However, suitable models which can account for the resonant coupling condition giving rise to pronounce multimode dynamics are currently not available. Finally, we point out that the demonstrated coherence properties of the system are highly interesting for novel technical and medical applications, such as in chaotic light detection and ranging applications [7] and coherence tomography [42]. For these applications, such bright, incoherent light sources with good beam properties are required.

ACKNOWLEDGMENTS

We gratefully acknowledge funding by the German Federal Ministry of Education and Research (BMBF) under Contract No. FK 13N8174 and thank Sacher Lasertechnik GmbH, Marburg, for fruitful collaboration and providing the LYNX system which served as the basis for development of this versatile and robust short-cavity SL system.

[1] *Fundamental Issues of Nonlinear Laser Dynamics*, edited by B. Krauskopf and D. Lenstra, AIP Conf. Proc. No. 548 (AIP, New York, 2000).
[2] C. H. Henry, IEEE J. Quantum Electron. **QE-18**, 259 (1982).
[3] J. Sacher, W. Elsäßer, and E. O. Göbel, Phys. Rev. Lett. **63**, 2224 (1989).
[4] T. Erneux, F. Rogister, A. Gavrielides, and V. Kovanis, Opt. Commun. **183**, 467 (2000).
[5] J. Mørk, B. Tromborg, and J. Mark, IEEE J. Quantum Electron. **QE-28**, 93 (1992).
[6] G. C. Dente, P. S. Durkin, K. A. Wilson, and C. E. Moeller, IEEE J. Quantum Electron. **QE-24**, 2441 (1988).
[7] F. Y. Lin and H. M. Liu, IEEE J. Sel. Top. Quantum Electron. **STQE-10**, 991 (2004).
[8] C. R. Phys. **5** (6) (2004), special issue on cryptography using optical chaos, edited by L. Larger and J. P. Goedgebuer.
[9] IEEE J. Quantum Electron. **38** (9) (2002), feature section on optical chaos and applications to cryptography, edited by S. Donati and C. R. Mirasso.
[10] R. Lang and K. Kobayashi, IEEE J. Quantum Electron. **QE-16**, 347 (1980).
[11] J. Mørk, B. Tromborg, and P. L. Christiansen, IEEE J. Quantum Electron. **QE-24**, 123 (1988).
[12] G. H. M. van Tartwijk, A. M. Levine, and D. Lenstra, IEEE J. Sel. Top. Quantum Electron. **STQE-1**, 466 (1995).
[13] T. Heil, I. Fischer, W. Elsäßer, and A. Gavrielides, Phys. Rev. Lett. **87**, 243901 (2001).
[14] T. Heil, I. Fischer, and W. Elsäßer, Phys. Rev. A **60**, 634 (1999).
[15] D. Lenstra, Quantum Semiclassic. Opt. **9**, U3 (1997).
[16] I. Fischer, G. H. M. vanTartwijk, A. M. Levine, W. Elsäßer, E. Göbel, and D. Lenstra, Phys. Rev. Lett. **76**, 220 (1996).
[17] A. T. Ryan, G. P. Agrawal, G. R. Gray, and E. C. Gage, IEEE J. Quantum Electron. **QE-30**, 668 (1994).
[18] D. W. Sukow, T. Heil, I. Fischer, A. Gavrielides, A. Hohl-AbiChedid, and W. Elsäßer, Phys. Rev. A **60**, 667 (1999).
[19] F. Rogister, P. Megret, O. Deparis, and M. Blondel, Phys. Rev. A **62**, 061803(R) (2000).
[20] C. L. Tang, H. Statz, and G. deMars, J. Appl. Phys. **34**, 2289 (1963).
[21] E. A. Viktorov and P. Mandel, Opt. Lett. **22**, 1568 (1997).
[22] T. W. Carr, D. Pieroux, and P. Mandel, Phys. Rev. A **63**, 033817 (2001).
[23] M. Yousefi, A. Barsella, D. Lenstra, G. Morthier, R. Baets, S. McMurtry, and J. P. Vilcot, IEEE J. Quantum Electron. **QE-39**, 1229 (2003).

[24] P. Mandel, E. A. Viktorov, C. Masoller, and M. S. Torre, Physica A **327**, 129 (2003).
[25] I. V. Koryukin and P. Mandel, Phys. Rev. A **70**, 053819 (2004).
[26] M. Homar, S. Balle, and M. SanMiguel, Opt. Commun. **131**, 380 (1996).
[27] B. Tromborg, J. Mørk, and V. Velichansky, Quantum Semiclassic. Opt. **9**, 831 (1997).
[28] A. A. Duarte and H. G. Solari, Opt. Commun. **144**, 99 (1997).
[29] M. Münkel, F. Kaiser, and O. Hess, Phys. Rev. E **56**, 3868 (1997).
[30] J. K. White and J. V. Moloney, Phys. Rev. A **59**, 2422 (1999).
[31] M. Möhrle, B. Sartorius, C. Bornholdt, S. Bauer, O. Brox, A. Sigmund, R. Steingrüber, M. Radziunas, and H. J. Wünsche, IEEE J. Sel. Top. Quantum Electron. **STQE-7**, 217 (2001).
[32] I. D. Henning and J. V. Collins, Electron. Lett. **19**, 927 (1983).
[33] C. H. Henry and R. F. Karzarinov, IEEE J. Quantum Electron. **QE-20**, 733 (1984).
[34] D. Marcuse and T. P. Lee, IEEE J. Quantum Electron. **QE-20**, 166 (1984).
[35] L. Furfaro, F. Pedaci, M. Giudici, X. Hachair, J. Tredicce, and S. Balle, IEEE J. Quantum Electron. **QE-40**, 1365 (2004).
[36] A. M. Yacomotti, L. Furfaro, X. Hachair, F. Pedaci, M. Giudici, J. Tredicce, J. Javaloyes, S. Balle, E. A. Viktorov, and P. Mandel, Phys. Rev. A **69**, 053816 (2004).
[37] M. J. Feigenbaum, Phys. Lett. **74A**, 375 (1979).
[38] T. Heil, I. Fischer, W. Elsäßer, B. Krauskopf, K. Green, and A. Gavrielides, Phys. Rev. E **67**, 066214 (2003).
[39] M. R. Daza, A. Tarun, K. Fujita, and C. Saloma, Opt. Commun. **161**, 123 (1999).
[40] C. Serrat, S. Prins, and R. Vilaseca, Phys. Rev. A **68**, 053804 (2003).
[41] C. Szwaj, S. Bielawski, D. Derozier, and T. Erneux, Phys. Rev. Lett. **80**, 3968 (1998).
[42] M. E. Brezinski and J. G. Fujimoto, IEEE J. Sel. Top. Quantum Electron. **STQE-5**, 1185 (1999).
[43] W. Elsäßer, Appl. Phys. Lett. **48**, 1323 (1986).
[44] P. Mandel, B. A. Nguyen, and K. Otsuka, Quantum Semiclassic. Opt. **9**, 365 (1997).
[45] G. Vaschenko, M. Giudici, J. J. Rocca, C. S. Menoni, J. R. Tredicce, and S. Balle, Phys. Rev. Lett. **81**, 5536 (1998).
[46] A. Uchida, Y. Liu, I. Fischer, P. Davis, and T. Aida, Phys. Rev. A **64**, 023801 (2001).
[47] J. M. Buldú, F. Rogister, J. Trull, C. Serrat, M. C. Torrent, J. Garcia-Ojalvo, and C. R. Mirasso, J. Opt. B: Quantum Semiclassical Opt. **4**, 415 (2002).
[48] C. Masoller, M. S. Torre, and P. Mandel, Phys. Rev. A **71**, 013818 (2005).
[49] K. Otsuka and Y. Aizawa, Phys. Rev. Lett. **72**, 2701 (1994).